A point vortex model for the formation of ocean eddies by flow separation

O. R. Southwick, E. R. Johnson, and N. R. McDonald

Citation: Physics of Fluids (1994-present) **27**, 016604 (2015); doi: 10.1063/1.4906112
View online: http://dx.doi.org/10.1063/1.4906112
View Table of Contents: http://scitation.aip.org/content/aip/journal/pof2/27/1?ver=pdfcov
Published by the AIP Publishing

PHYSICS OF FLUIDS **27**, 016604 (2015)

A point vortex model for the formation of ocean eddies by flow separation

O. R. Southwick,[a] E. R. Johnson,[b] and N. R. McDonald[c]
Department of Mathematics, University College London, London WC1E 6BT, United Kingdom

(Received 1 September 2014; accepted 6 January 2015; published online 21 January 2015)

A simple model for the formation of ocean eddies by flow separation from sharply curved horizontal boundary topography is developed. This is based on the Brown–Michael model for two-dimensional vortex shedding, which is adapted to more realistically model mesoscale oceanic flow by including a deforming free surface. With a free surface, the streamfunction for the flow is not harmonic so the conformal mapping methods used in the standard Brown–Michael approach cannot be used and the problem must be solved numerically. A numerical scheme is developed based on a Chebyshev spectral method for the streamfunction partial differential equation and a second order implicit timestepping scheme for the vortex position ordinary differntial equations. This method is used to compute shed vortex trajectories for three background flows: (A) a steady flow around a semi-infinite plate, (B) a free vortex moving around a semi-infinite plate, and (C) a free vortex moving around a right-angled wedge. In (A), the inclusion of surface deformation dramatically slows the vortex and changes its trajectory from a straight path to a curved one. In (B) and (C), without the inclusion of flow separation, free vortices traverse fully around the tip along symmetrical trajectories. With the effects of flow separation included, very different trajectories are found: for all values of the model parameter—the Rossby radius—the free and shed vortices pair up and move off to infinity without passing around the tip. Their final propagation angle depends strongly and monotonically on the Rossby radius. [http://dx.doi.org/10.1063/1.4906112]

I. INTRODUCTION

Eddies play an important role in oceanic circulation by transporting significant amounts of heat, salt, mass, and momentum. Those on the mesoscale (~10–500 km in diameter) can be highly coherent features with lifespans of months, or even years, enabling them to travel across entire ocean basins. While large enough to be significant, these eddies are small enough to be difficult to resolve in global ocean models. Indeed, all such models must include a parameterisation of the effects of eddies at some scale. Therefore, an improved understanding of the generation and dynamics of eddies is important for further improvement in large scale ocean modelling. One aspect of this must be an understanding of the dynamics of eddies in the presence of topographic features. Long-lived eddies have been observed to interact with topographic features such as islands, mid-ocean ridges, and sea-mounts. The North Brazil Current rings, which contribute substantially to the Atlantic meridional overturning circulation,[1] often interact with the islands of the Lesser Antilles.[2] Typically, they either disintegrate upon collision or pass between the islands. As such, they have received significant theoretical, observational, numerical, and experimental attention.[3,4] Another example is the lenses of dense, salty water of Mediterranean origin known

[a]oliver.southwick.11@ucl.ac.uk
[b]e.johnson@ucl.ac.uk
[c]n.r.mcdonald@ucl.ac.uk

as "meddies," which propagate deep in the North Atlantic and are observed to frequently interact with sea-mounts.[5]

The simplest approach to modelling ocean eddies is to consider a constant-depth barotropic ocean with point vortices and topography extending vertically through the entire fluid depth. The flow dynamics then evolve according to the two-dimensional Euler equations. This model enables significant analytical progress with complex variable methods and has been used in a number of works which consider different configurations of topography. Johnson and McDonald used conformal mapping techniques to construct the vortex Hamiltonian (Kirchoff–Routh path function) for a point vortex and compared it to the motion of an initially circular vortex patch in various domains: a single gap in a wall,[6] two circular islands,[7] multiple circular islands using the point island approximation,[8] and a wall with multiple gaps.[9] They found that the centroid of the patch very closely followed the trajectory of a point vortex except when the patch deformed significantly, as it does, for example, when it approaches a horizontal boundary. Crowdy and Marshall derived the vortex Hamiltonian for N point vortices in multiply connected domains[10] and applied it to find point vortex trajectories around multiple circular islands[11] and vortex trajectories in more general multiply connected slit domains by conformally mapping them to circular domains.[12] These techniques have also been applied to vortex motion on a sphere with boundaries.[13]

While this model enables a large number of exact solutions, in many oceanographic contexts, it may be appropriate to include the effect of surface deformation. This surface could either be a fluid–air interface or the interface between two layers of different densities. Surface deformation is modelled using the quasigeostrophic (QG) flow equations and has a single parameter: the Rossby radius of deformation (or simply "Rossby radius"), which is the lengthscale over which surface perturbations decay. A constant depth fluid is the limiting case when the Rossby radius goes to infinity and is often referred to as the "rigid-lid limit." From here onward, fluid with finite Rossby radius will be referred to simply as a quasigeostrophic or QG flow, and constant depth fluid (i.e., infinite Rossby radius flow) will be referred to as rigid-lid fluid. QG flow is not harmonic so the complex variable methods previously applied cannot be used, meaning that exact solutions are difficult to find and numerical approaches must be employed instead. Nilawar, Johnson, and McDonald[14] considered the motion of a point vortex approaching a gap in a wall for QG flow. For various Rossby radii, they calculated point vortex trajectories numerically using boundary integral methods and compared them to the motion of vortex patches computed with contour dynamics. They found that with lower Rossby radius, the vortices were more likely to pass through the gap.

Many of the shapes of topography previously considered (e.g., semi-infinite plates, gaps in walls and wedges) feature sharp corners representing sharply curving boundary topography. In these situations, without viscosity, the flow field typically becomes singular at the boundary corners. In reality, this unphysical effect is prevented by flow separation at the sharp corner. Flow at large Reynolds number around obstacles—especially obstacles with a sharp point—typically separates, shedding the viscous boundary layer out into the flow. This shed fluid has high vorticity and rolls up into a concentrated core: a shed vortex.

Ocean eddies created by flow separation have frequently been observed around islands such as the Canaries[15] and Izu Islands[16] and capes such as Cape Ann.[17] These eddies are often mesoscale[17–19] and their dynamics can be effected by rotation (away from the equator)[19] and stratification. They are of significant biological—as well as physical—interest as they can cause strong upwelling and increased levels of chlorophyll and phytoplankton production: the "island mass effect."[20] Topographic forcing of the oceanic flow has been shown to be the main mechanism for the eddy generation—with wind shear acting as an additional supporting source of vorticity—in observational[15] and numerical[21] investigations of eddy generation from Gran Canaria. As such, the formation of eddies by flow separation has received significant observational, experimental, and numerical attention. The stability of general island wakes in the flow of rotating, stratified, shallow water has been studied experimentally using the three-dimensional LEGI Coriolis platform.[22] Numerical investigations have often aimed to realistically capture the full complexity of the flow with relatively complex models. For example, the wake of the ocean flow past the Madeira archipelago was recently investigated using a three-dimensional primitive equation model with realistic bathymetry.[23] It would be complementary to these approaches to develop a simplified

model that captures the key features of the flow but which is easier to implement and understand. A model which isolates the key physical process in a simple way will benefit understanding and aid interpretation of the results of more complex models, experiments, and observations. Additionally, such a model will have the significant extra benefit of being much cheaper to implement numerically than more complex approaches.

A simple approach modelling the formation of vortices by flow separation is the Brown–Michael model.[24] Brown and Michael refined calculations of lift on an aeroplane delta wing by including the lift generated by the vortex sheet shed from the trailing edge. Their model replaces the spiral vortex sheet—both the shape and strength of which must be determined—by a single point vortex of variable circulation. This key step simplifies the problem dramatically from solving partial differential equations (PDEs) governing the vortex sheet evolution, which may have issues of ill-posedness and instability at arbitrarily small wavelengths and so require regularisation.[25] The point vortex formulation inevitably leaves a pressure discontinuity across a branch cut connecting the vortex to the separation point, which is interpreted as being the infinitesimal connecting sheet along which vorticity is fed to the shed vortex. Brown and Michael derived a new equation of motion for the vortex—the Brown–Michael equation—which ensured the net force, on the cut and vortex combined, was zero.

In addition to continued use in studies of aerofoils,[26] the Brown–Michael model has been used in a range of applications to model high Reynolds number flow separation, e.g., various coupled solid–fluid interactions involving shedding such as a falling playing card or a flapping flag.[27–29] The performance of the Brown–Michael model has been examined in a number of studies. It was compared to a vortex sheet method and a penalised Navier–Stokes method in a model of the wake produced by a swimming fish.[30] The wake structures produced by the three methods were qualitatively similar (as shown in their Figs. 2–4), and the shed circulation and drag coefficient were of the same order of magnitude but with more significant differences across the three methods. A comparison between the Brown–Michael method and a more sophisticated numerical solution of the Navier–Stokes equations using a viscous vortex particle method showed good qualitative agreement in an investigation of flow separation over a rapidly pitching plate.[31] In both of these studies, the Brown–Michael approach is of negligible computational cost in comparison to the more sophisticated methods. There have also been developments on the model itself. Cortelezzi solved the equation of motion for a vortex shed from a semi-infinite plate[32] for any free-stream condition and derived a time-dependent scaling that collapses all solutions onto the impulsively started case. Howe studied sound generated by a vortex translating around a semi-infinite plate[33] and proposed an emended Brown–Michael equation where the vortex motion is set to cancel not only the net force but also a previously unbalanced reaction force caused by the residual couple.

Here, aiming to improve oceanic flow models, a new version of the Brown–Michael equation for QG flow is derived in Sec. II. With QG flow, complex variable methods enabling construction of the vortex Hamiltonian in conformally mapped domains are no longer available, so instead numerical techniques will be employed. In Sec. III, a numerical scheme based on a Chebyshev spectral method to solve the PDE for the streamfunction and a second order implicit scheme to integrate the Brown–Michael coupled ordinary differntial equations (ODEs) is developed. In Sec. IV, this method is applied to three background flows: (A) a steady flow around a semi-infinite plate, (B) a free vortex moving around a semi-infinite plate, and (C) a free vortex moving around a right-angled wedge.

II. DERIVATION OF A QUASIGEOSTROPHIC BROWN–MICHAEL EQUATION

In the Brown–Michael model, the spiral vortex sheet formed from a separated flow is modelled by a single point vortex of variable circulation. The circulation of the shed vortex is set to ensure no velocity singularity at the separation point. This is known as the Kutta condition. However, the model has the problem that, due to the varying circulation, there is an unphysical pressure discontinuity along some line (a branch cut) connecting the vortex to the separation point. Brown and Michael's solution to this problem is to require that the vortex moves relative to the fluid around it, so that it experiences a lift force which cancels out the net force on the vortex and cut combined.

Here, this model will be adapted for QG flow using a new derivation based on the streamfunction instead of the complex potential.

A. Quasigeostrophic flow

Consider a shallow layer of fluid in a rotating reference frame with non-dimensional free surface deviation η. The flow satisfies the non-dimensional rotating shallow water equations

$$\varepsilon \frac{\mathrm{D}\boldsymbol{u}}{\mathrm{D}t} + \hat{\boldsymbol{e}}_z \wedge \boldsymbol{u} = -\nabla\eta, \tag{1a}$$

$$\varepsilon \frac{\mathrm{D}\eta}{\mathrm{D}t} + \left(a^2 + \varepsilon\eta\right)\nabla \cdot \boldsymbol{u} = 0, \tag{1b}$$

for small ε, the Rossby number.[34] These are equations in the (x, y)-plane where $\boldsymbol{u}$ is the horizontal velocity, $\hat{\boldsymbol{e}}_z$ is the unit vector in the z-direction, and $a = L_R/L$ is the ratio of the Rossby radius $L_R = \sqrt{g'D}/f_0$ (for reduced gravity g', typical fluid depth D, and Coriolis parameter f_0) to the typical horizontal lengthscale L. An asymptotic expansion of the form $\eta = \eta_0 + \epsilon\eta_1 + \cdots$ gives at leading order

$$\boldsymbol{u}_0 = -\nabla \wedge (\eta_0 \hat{\boldsymbol{e}}_z) \tag{2}$$

and at $O(\varepsilon)$

$$\frac{\mathrm{D}_0\boldsymbol{u_0}}{\mathrm{D}_0 t} + \hat{\boldsymbol{e}}_z \wedge \boldsymbol{u}_1 = -\nabla\eta_1, \tag{3a}$$

$$\frac{1}{a^2}\frac{\mathrm{D}_0\eta_0}{\mathrm{D}_0 t} + \nabla \cdot \boldsymbol{u}_1 = 0, \tag{3b}$$

where $\mathrm{D}_0/\mathrm{D}_0 t = \partial/\partial t + (\boldsymbol{u}_0 \cdot \nabla)$. Taking the curl of (3a) and substituting in (3b) gives

$$\frac{\mathrm{D}_0}{\mathrm{D}_0 t}\left(\nabla^2\eta_0 - \frac{1}{a^2}\eta_0\right) = 0. \tag{4}$$

Equation (4) implies that the potential vorticity $q_0 = \nabla^2\eta_0 - \eta_0/a^2$ is conserved following the leading order flow. In the situations considered here, any topography extends vertically throughout the entire fluid depth and the flow is initially irrotational so $q_0 = 0$, except at the positions of any point vortices which give delta function singularities of potential vorticity. That is, for a point vortex of strength Γ at position $\boldsymbol{x}_\mathrm{v}$,

$$\nabla^2\eta_0 - \frac{1}{a^2}\eta_0 = \Gamma\delta(\boldsymbol{x} - \boldsymbol{x}_\mathrm{v}). \tag{5}$$

B. The Brown–Michael correction

Consider a point vortex of time dependent circulation $\Gamma = \Gamma(t)$ at the origin. At leading-order the streamfunction satisfies (5) and is given by $\eta_0 = (-\Gamma/2\pi)K_0(r/a)$, where K_n is the modified Bessel function of the second kind of order n. As the flow around the vortex is purely azimuthal, $\boldsymbol{u}_0 = u_{0\theta}\hat{\boldsymbol{e}}_\theta$ and $\boldsymbol{u}_1 = u_{1\theta}\hat{\boldsymbol{e}}_\theta$, so the azimuthal component of (3a) is

$$\frac{\partial u_{0\theta}}{\partial t} = -\frac{1}{r}\frac{\partial\eta_1}{\partial\theta}. \tag{6}$$

The leading order azimuthal velocity is given by $u_{0\theta} = \partial\eta_0/\partial r = \Gamma/(2\pi a)K_1(r/a)$. Substituting this into (6) and integrating with respect to θ gives

$$\eta_1 = -\frac{\dot{\Gamma}}{2\pi}\frac{r}{a}K_1\left(\frac{r}{a}\right)\theta + \hat{\eta}(r) \tag{7}$$

for some function $\hat{\eta}(r)$, where the dot denotes a time derivative. Therefore, there is a pressure discontinuity of size $(\dot{\Gamma}r/a)K_1(r/a)$ across some branch cut. In the rigid-lid problem considered

by Brown and Michael, the pressure discontinuity was constant along the cut so the net force on the cut was independent of the cut shape. For quasigeostrophic dynamics, this is not the case and the net force on the cut does depend on its shape. Here, a straight line connecting the vortex to the separation point is used for the cut shape since this minimises the total force exerted on the cut. Calculations using cuts with large perturbations of symmetric quadratic shape and maximum displacement as large as half of the cut length have been performed. These give net forces with less than a tenth maximum difference in magnitude and vortex trajectories with less than 4% difference in position. It is also worth noting that this correction term is not the main effect in the dynamics of the problem. In the original rigid-lid Brown–Michael problem, the effect of the correction term is to reduce the shed vortex speed by a third and it has no effect on the final shape of the trajectory. With a linear cut and in the frame with the separation point at the origin and the shed vortex at $\boldsymbol{x}_\mathrm{s}$, the net force on the cut is

$$\boldsymbol{F}_\mathrm{net} = -\dot{\Gamma}\int_0^{|\boldsymbol{x}_\mathrm{s}|} \frac{r}{a} K_1\left(\frac{r}{a}\right) \mathrm{d}r\, \boldsymbol{n}, \tag{8}$$

where $\boldsymbol{n} = (\hat{\boldsymbol{e}}_z \wedge \boldsymbol{x}_\mathrm{s})/|\boldsymbol{x}_\mathrm{s}|$ is the unit normal to the cut.

The Brown–Michael model requires the vortex to move such that its lift cancels the net pressure discontinuity. Treating the vortex as a cylinder with infinitesimal radius (equivalent to the rigid-lid limit), the Kutta–Joukowski lift theorem[35] shows that a vortex moving at velocity $\dot{\boldsymbol{x}}_\mathrm{s}$ in a flow with velocity $\widetilde{\boldsymbol{u}}$ experiences the lift force

$$\boldsymbol{F}_\mathrm{lift} = \Gamma \hat{\boldsymbol{e}}_z \wedge (\widetilde{\boldsymbol{u}}(\boldsymbol{x}_\mathrm{s}) - \dot{\boldsymbol{x}}_\mathrm{s})\,. \tag{9}$$

$\widetilde{\boldsymbol{u}}(\boldsymbol{x}_\mathrm{s})$ is the velocity a "free" vortex would have, i.e., the velocity due to the background flow and the interaction of the vortex with the domain boundary, but excluding the direct contribution from the vortex itself. Balancing this lift force with the total pressure discontinuity gives the quasigeostrophic Brown–Michael (QGBM) equation

$$\dot{\boldsymbol{x}}_\mathrm{s} = \widetilde{\boldsymbol{u}}(\boldsymbol{x}_\mathrm{s}) - \frac{\dot{\Gamma}}{\Gamma}\frac{\boldsymbol{x}_\mathrm{s}}{|\boldsymbol{x}_\mathrm{s}|}\int_0^{|\boldsymbol{x}_\mathrm{s}|} \frac{r}{a} K_1\left(\frac{r}{a}\right) \mathrm{d}r. \tag{10}$$

The system is closed by the Kutta condition, which requires that the vortex circulation Γ is such that there is no velocity singularity at the origin, i.e., that $\widetilde{\boldsymbol{u}}(\boldsymbol{x} = \boldsymbol{0}) = \boldsymbol{0}$.

The equation of motion of a free vortex (i.e., a vortex with constant circulation) with position $\boldsymbol{x}_\mathrm{f}$ is

$$\dot{\boldsymbol{x}}_\mathrm{f} = \widetilde{\boldsymbol{u}}(\boldsymbol{x}_\mathrm{f}). \tag{11}$$

This is equal to QGBM equation (10) with $\dot{\Gamma} = 0$. In the rigid-lid limit $a \to \infty$, the QGBM equation reduces to the original Brown–Michael equation

$$\dot{\boldsymbol{x}}_\mathrm{s} = \widetilde{\boldsymbol{u}}(\boldsymbol{x}_\mathrm{s}) - \frac{\dot{\Gamma}}{\Gamma}\boldsymbol{x}_\mathrm{s}. \tag{12}$$

Here, $\widetilde{\boldsymbol{u}}(\boldsymbol{x}_\mathrm{s})$ is again the velocity a free vortex would have but now in rigid-lid flow.

From here onward, only the leading order motion will be considered so subscripts are dropped, e.g., η is written for η_0. The streamfunction will be split into two components $\eta = \widetilde{\eta} + \eta_\mathrm{v}$, where η_v is the direct contribution from any vortices ignoring boundaries and is known and $\widetilde{\eta}$ is the rest of the solution which is to be found. $\widetilde{\eta}$ has zero potential vorticity and ensures that the no flux boundary condition for η is satisfied. It satisfies the modified Helmholtz equation

$$\nabla^2\widetilde{\eta} - \frac{1}{a^2}\widetilde{\eta} = 0. \tag{13}$$

III. NUMERICAL SCHEME

A. Physical problem and numerical procedure

The physical problems considered here all feature a wedge of angle α ($0 \le \alpha < 2\pi$) with the tip at the origin (as shown in Fig. 1(a)) and some background flow. Without shedding, and for $\alpha < \pi$,

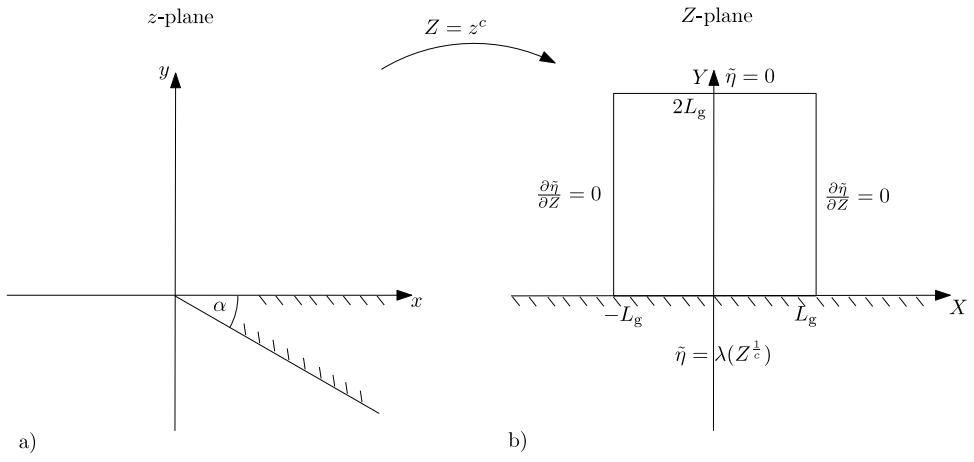

FIG. 1. Schematic of (a) the physical domain outside a wedge of angle α and (b) the mapped plane showing the extent of the computational domain containing the Chebyshev grid (for $\alpha \neq 0$) and showing the boundary conditions applied in the numerical scheme. The mapping coefficient is $c = \pi/(\pi - \alpha)$.

a general background flow would give a velocity singularity at the wedge tip. This is unphysical so, instead, a vortex is shed to ensure there is no velocity singularity at the tip. This shed vortex will start from the tip and move according to (10). Three specific examples will be considered here. The first two are for a semi-infinite plate (a wedge of angle $\alpha = 0$), first with a steady background flow (a flow with boundary condition η = constant on the plate) and second with a free vortex as the background flow. The third example is a wedge of angle $\alpha = \pi/2$ and a free vortex as the background flow.

The positions of the shed vortex and any free vortices evolve according to the simple ODEs (10) and (11), which can be solved using standard finite difference methods. A greater challenge is finding the value of the terms in these ODEs. In particular, $\widetilde{\boldsymbol{u}}(\boldsymbol{x}_\mathrm{s})$ and Γ in (10) and the velocity the free vortex $\widetilde{\boldsymbol{u}}(\boldsymbol{x}_\mathrm{f})$ in (11). These all depend on the streamfunction $\widetilde{\eta}$, which is the solution of the modified Helmholtz equation (13), a second order elliptic PDE. The numerical procedure employed here will be, at each point in time, to solve the PDE for the streamfunctions for the background flow and the flow due to the shed vortex and use these to compute $\widetilde{\boldsymbol{u}}(\boldsymbol{x}_\mathrm{s})$, Γ, and the velocity of any free vortices. This gives all the terms in the ODEs, which can then be solved using an implicit finite difference scheme.

A good first choice for solving PDE (13) with boundary conditions only specified on the wedge boundaries and at infinity is a boundary integral method.[14] However, derivatives of the streamfunction near the origin have a $|\boldsymbol{x}|^{(\alpha-\pi)/(2\pi-\alpha)}$ singularity, and the implementation of the Kutta condition requires the coefficient of this singularity to be computed accurately. This is a significant challenge for the boundary integral method. An alternative, which deals effectively with the singularity problem, is to conformally map the problem to the upper half-plane as shown in Fig. 1. Now, the singularity is contained explicitly in the mapping, and derivatives are bounded. However, the mapping has changed the form of the PDE, and the open domain Green's function is not known, so a boundary integral method cannot be used. The half-plane geometry in the mapped plane suggests using a grid based method, e.g., a finite difference or Chebyshev spectral method. Both of these methods using mapping had improved accuracy at the tip compared to the boundary integral method. The spectral method had the highest accuracy and the strongest convergence of all three methods for comparable computation times, so was selected.

B. Spectral method for finding $\widetilde{\eta}$

The leading order surface deformation $\widetilde{\eta}$ is the solution of the problem

$$\nabla^2\widetilde{\eta} - \frac{1}{a^2}\widetilde{\eta} = 0, \tag{14}$$

with boundary conditions

$$\widetilde{\eta} = \widetilde{\eta}_{\mathrm{b}}(\boldsymbol{x}), \qquad \text{for } \theta = 0,\ 2\pi - \alpha, \tag{15a}$$

$$\widetilde{\eta} \to 0, \qquad \text{as } r \to \infty, \tag{15b}$$

for some function $\widetilde{\eta}_{\mathrm{b}}(\boldsymbol{x})$, where (r,θ) are the polar coordinates of $\boldsymbol{x}$. (15a) ensures that the wedge is bounded by a streamline, so there is no flow through it. The physical problem being considered determines $\widetilde{\eta}_{\mathrm{b}}(\boldsymbol{x})$. For a steady flow anti-clockwise around the wedge $\widetilde{\eta}_{\mathrm{b}}(\boldsymbol{x}) = -1$ and for a vortex of unit strength at position $\boldsymbol{x}_{\mathrm{s}}$, the boundary condition on the wedge is $\widetilde{\eta}_{\mathrm{b}}(\boldsymbol{x}) = K_0(|\boldsymbol{x} - \boldsymbol{x}_{\mathrm{s}}|)/2\pi$. Derivatives of the solution to this problem have a $|\boldsymbol{x}|^{(\alpha-\pi)(2\pi-\alpha)}$ singularity at the origin, the coefficient of which must be found to satisfy the Kutta condition. This singularity is treated separately—avoiding its numerical difficulties—by conformally mapping to the upper half-plane with the map $Z = z^c$, where $c = \pi/(2\pi - \alpha)$, for physical domain coordinates $z = x + \mathrm{i}y = r\mathrm{e}^{\mathrm{i}\theta}$ and mapped plane coordinates $Z = X + \mathrm{i}Y = R\mathrm{e}^{\mathrm{i}\Theta}$. Now, derivatives in the physical domain are related to those in the mapped domain by

$$\begin{pmatrix} \dfrac{\partial\widetilde{\eta}}{\partial x} \\ \dfrac{\partial\widetilde{\eta}}{\partial y} \end{pmatrix} = \frac{c}{R^m} \begin{pmatrix} \cos m\Theta & -\sin m\Theta \\ \sin m\Theta & \cos m\Theta \end{pmatrix} \begin{pmatrix} \dfrac{\partial\widetilde{\eta}}{\partial X} \\ \dfrac{\partial\widetilde{\eta}}{\partial Y} \end{pmatrix}, \tag{16}$$

where $m = (\pi - \alpha)/\pi$, so the singularity is contained explicitly in the mapping and mapped plane derivatives are bounded at $X = Y = 0$. The modified Helmholtz equation (14) in the mapped plane is

$$\nabla^2\widetilde{\eta} - \frac{|Z^{2m}|}{c^2a^2}\widetilde{\eta} = 0, \tag{17}$$

where $\nabla^2 = \partial^2/\partial X^2 + \partial^2/\partial Y^2$, with boundary conditions appropriately changed as follows.

The PDE is solved using a Chebyshev spectral method with N^2 grid points. For general α, it is solved on the square $-L_{\mathrm{g}} < X < L_{\mathrm{g}}$, $0 < Y < 2L_{\mathrm{g}}$ as shown in Fig. 1(b), but for $\alpha = 0$, the symmetry across the Y-axis can be exploited and the domain $0 < X < L_{\mathrm{g}}$, $0 < Y < 2L_{\mathrm{g}}$ is used. The boundary condition on the X-axis is

$$\widetilde{\eta} = \widetilde{\eta}_{\mathrm{b}}(Z^{\frac{1}{c}}), \qquad \text{for } Y = 0. \tag{18}$$

The far-field boundary conditions are imposed on the other sides of the square. These are approximate for a finite numerical domain so introduce an error exponentially small in L_{g}/a. The boundary conditions become exact in the limit $L_{\mathrm{g}}/a \to \infty$, and the effect of the error introduced decays exponentially away from the boundary. On the top, this gives

$$\widetilde{\eta} = 0, \qquad \text{for } Y = 2L_{\mathrm{g}}, \tag{19}$$

and on the sides, it is

$$\frac{\partial\widetilde{\eta}}{\partial X} = 0, \qquad \text{for } X = \pm L_{\mathrm{g}}, \tag{20}$$

for general α, or

$$\frac{\partial\widetilde{\eta}}{\partial X} = 0, \qquad \text{for } X = 0,\ L_{\mathrm{g}}, \tag{21}$$

for $\alpha = 0$. When $\alpha = 0$, the boundary condition on $X = 0$ is in fact exact, by symmetry.

Solving (17) with boundary conditions(18)–(20) or (21) with a spectral method yields a solution on the grid from which derivatives can be calculated spectrally at any point and used to find derivatives in the physical plane via (16). The Kutta condition can be implemented by finding $\partial\widetilde{\eta}/\partial Y(0,0)$ both for the background flow and for a vortex of unit strength. For the special case of a semi-infinite plate ($\alpha = 0$) and constant boundary condition, say $\widetilde{\eta}_{\mathrm{b}}(x) = -1$, the numerical results indicate that the solution along the Y-axis is $\widetilde{\eta}(0,Y) = -\mathrm{erfc}(Y/\sqrt{a})$, the complementary error function, as shown in Appendix A. This simplifies the implementation of the Kutta condition in this case.

C. Timestepping scheme for the QGBM equation

The $\dot{\Gamma}$ term in the QGBM equation suggests an implicit scheme over an explicit one, since the latter can only calculate $\dot{\Gamma}$ with a lag. For convenience, rewrite the QGBM equation (10) as

$$\dot{x} = u + f\dot{\Gamma}, \tag{22a}$$

$$\dot{y} = v + g\dot{\Gamma}, \tag{22b}$$

where $\boldsymbol{x}_\mathrm{s} = (x_\mathrm{s}, y_\mathrm{s})^\top$ and $\widetilde{\boldsymbol{u}}(\boldsymbol{x}_\mathrm{s})$ are rewritten as $\boldsymbol{x} = (x, y)^\top$ and $(u, v)^\top$, respectively, and

$$(f, g)^\top = -\frac{\boldsymbol{x}}{|\boldsymbol{x}|\Gamma}\int_0^{|\boldsymbol{x}|} \frac{r}{a} K_1\left(\frac{r}{a}\right)\,\mathrm{d}r. \tag{23}$$

Given the shed vortex position, the spectral method can be used to compute u, v, and Γ (via the Kutta condition), then f and g follow straightforwardly from (23). The QGBM equation is discretised using a second order central difference scheme

$$\frac{x_{n+1} - x_n}{h} = \frac{u_{n+1} + u_n}{2} + \left(\frac{f_{n+1} + f_n}{2}\right)\left(\frac{\Gamma_{n+1} - \Gamma_n}{h}\right), \tag{24a}$$

$$\frac{y_{n+1} - y_n}{h} = \frac{v_{n+1} + v_n}{2} + \left(\frac{g_{n+1} + g_n}{2}\right)\left(\frac{\Gamma_{n+1} - \Gamma_n}{h}\right), \tag{24b}$$

with timestep h. This is a widely used implicit finite difference method with good accuracy and improved stability over an explicit scheme. This gives a non-linear root finding problem, $\boldsymbol{F}(x_{n+1}, y_{n+1}) = 0$, for x_{n+1}, y_{n+1} which is solved with Broyden's method.[36] In the Broyden's method calculation, a first order explicit approximation is used for the initial guess of (x_{n+1}, y_{n+1}), the known rigid-lid solution (obtained via conformal mapping) for $\dot{\Gamma}$ is used at the first timestep, and a first order approximation is used for the Jacobian matrix of $\boldsymbol{F}(x_{n+1}, y_{n+1})$ on the first iteration.

D. Practicalities for the numerical scheme

In addition to a description of the main scheme, there are some practical details that merit description. First, in the case with a free vortex present as well as the shed vortex, there is a second pair of ODEs, $\dot{\boldsymbol{x}}_\mathrm{f} = \boldsymbol{u}_\mathrm{f}$, to solve. These are also discretised using a central difference scheme and there are now four unknowns to be found using Broyden's method. Second, in the numerical scheme, it is not possible for a vortex to be exactly at the tip of the wedge as this would give a singularity in $\widetilde{\eta}_\mathrm{b}(\boldsymbol{x})$ at the tip. Therefore, an initial shed vortex position very close to the tip is used instead. Being close to the tip (i.e., much less than the lengthscale a) is equivalent to the rigid-lid limit so the initial condition used for the shed vortex position $(x_{\mathrm{s}_0}, y_{\mathrm{s}_0})$ is a point along the rigid-lid trajectory. For a small distance from the tip (typically $\sim 10^{-2}a$ is used), this introduces a small error in the initial trajectory, of magnitude less than a tenth of the distance of the tip from the starting point. Furthermore, tests with vortices with various initial positions relax quickly to the same solution as shown in Fig. 2. That is, the vortex trajectory is insensitive to the choice of the initial location of the shed vortex. The test trajectories start evenly spaced on a circle surrounding the point $(0, -0.01)$ and are all therefore in the lower half-plane, consistent with the rigid-lid trajectory where the vortex is shed in the negative y-direction. In the tests, the initial error decreases very rapidly, dropping several orders of magnitude very quickly, then settling on a slower but still exponential decrease. Physically, this is primarily due to the restorative effect of the Kutta condition. Displacing a vortex from its trajectory changes its strength. This changes the size of the component of the vortex velocity due to the interaction between the vortex and the physical boundaries, which acts against the displacement. Overall, the error caused by the initial position is insignificant in determining the ultimate trajectory of the shed vortex. The speed of the vortices may change significantly over a trajectory so a variable timestep is used. The velocity scale is approximated by

$$\text{velocity scale} = \frac{1}{a}\max\left(K_1\left(\frac{2y_\mathrm{f}}{a}\right), \Gamma K_1\left(\frac{2y_\mathrm{s}}{a}\right), K_1\left(\frac{|\boldsymbol{x}_\mathrm{s} - \boldsymbol{x}_\mathrm{f}|}{a}\right)\right), \tag{25}$$

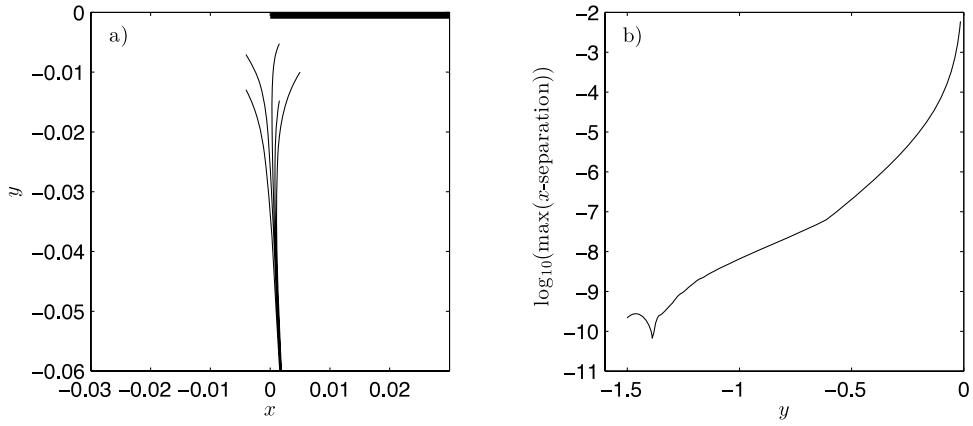

FIG. 2. (a) Trajectories for shed vortices starting at five different points then advancing following the quasigeostrophic Brown–Michael equation for a vortex shed from the tip of a semi-infinite plate under a steady flow. The five initial conditions are points equally spaced around a circle of radius 0.005 surrounding the point (0, −0.01), which will be used as the initial condition for later runs. (b) The base 10 logarithm of the maximum x-separation at fixed y of the five trajectories as a function of y. The trajectories differ by less than 10^{-8} at distances further than one Rossby radius from the plate.

i.e., as the maximum of the image velocity of the free or shed vortex or as the direct velocity exerted by the free vortex on the shed vortex. In the case of no free vortex, just the image of the shed vortex is used. The timestep is then scaled on 1/velocity scale. The size, L_g, of the spectral grid in the mapped plane is chosen such that the solution is always closer to the plate than to the boundaries with false boundary conditions.

E. Validation of the numerical scheme

A number of tests were used to validate the numerical scheme. In all cases, the results converge with increasing grid resolution N or grid size L_g (for constant N/L_g) and decreasing timestep h. For large a, the scheme is able to closely reproduce several rigid-lid results: a shed vortex trajectory for a steady background flow, close to the plate (Fig. 3); a free vortex trajectory around a semi-infinite plate (Fig. 5) or wedge; the velocity $\partial\widetilde{\eta}/\partial x(0, 0)$ (as required for the Kutta condition) for both a steady flow and a vortex around a semi-infinite plate; and the trajectories of a free and shed vortex around a semi-infinite plate (Fig. 6) and a wedge (Fig. 9). For a wedge with angle $\alpha = \pi$ (i.e., an infinite plate with a separation point specified at the origin) in QG flow, the ODEs for the vortex positions can be found exactly using the method of images. Integrating these using standard accurate Runge–Kutta methods (a fifth-order adaptive timestep Runge–Kutta Dormand–Prince method[37] implemented with MATLAB's ode45) gives a solution that matches that of the numerical scheme described here and also the rigid-lid solution when the free vortex is initially close to the plate. There are few analytical results to compare with in the limit $a \to 0$, aside from the trajectory of a free vortex around a semi-infinite plate which can also be closely reproduced (Fig. 5, the trajectory for $a = 0.01$ is barely distinguishable from the analytical result).

Although the convergence of the spectral method is good, a large number of grid points are needed in both the large a limit, where a large grid is needed to avoid the influence of the approximate boundary conditions, and in the small a limit, where many grid points are needed to resolve a sharply varying streamfunction. Hence—as well as for oceanographic relevance—the results considered will typically fall in the range $10^{-1} < a < 10^2$. All numerical results in this work have been run at a range of numerical parameters and compared with each other to ensure accuracy.

IV. RESULTS

A. Steady flow around a semi-infinite plate

The first example considered is vortex shedding owing to a steady background flow around a semi-infinite plate with boundary conditions $\eta = -1$ on the plate (all time-dependent cases can be

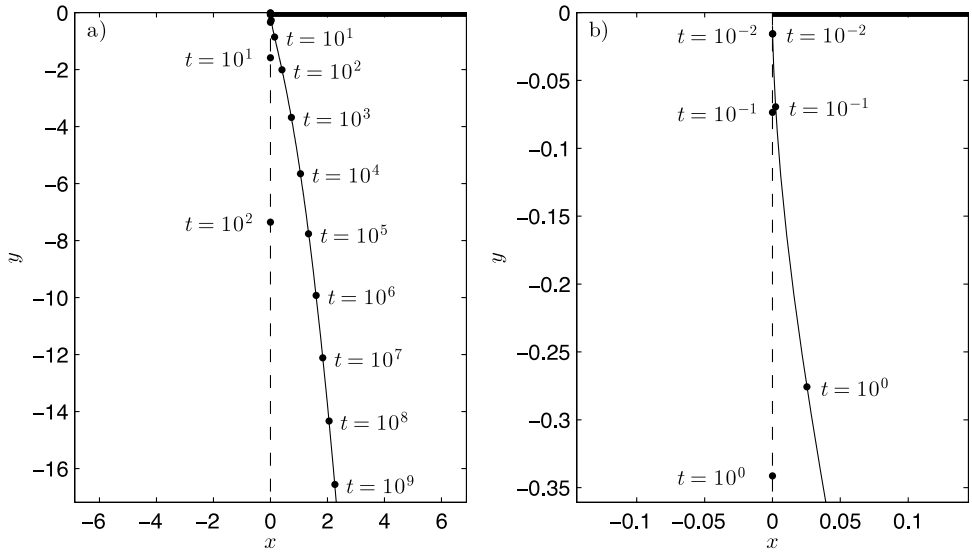

FIG. 3. Trajectories of Brown–Michael shed vortices for a steady flow around a semi-infinite plate. The QG ($a \neq 0$) solution (solid line) is computed numerically, and the rigid-lid ($a \to \infty$) solution (dashed) is exact. The plate is shown in dark along the positive x-axis. The two views are (a) the full solution and (b) a view focused on the origin, showing that the solutions are initially identical. The solution at various time points has been marked, demonstrating how much slower the QG vortex is. The initial position of the QG vortex was $(x_{s_0}, y_{s_0}) = (0, -0.01)$.

collapsed on to this through scaling time), $\eta \to 0$ at infinity and with no singularities (other than the shed vortex) in the flow. The exact solution[32] to the Brown-Michael vortex shedding problem in the rigid-lid limit (a flow with free-stream speed $-2/\sqrt{\pi}$ along the top of the plate) is a vortex shed perpendicular to the plate with trajectory

$$(x_s, y_s) = \left(0, -\frac{t^{\frac{2}{3}}}{2\pi^{\frac{1}{3}}}\right). \tag{26}$$

For the QG problem, there is no lengthscale other than the Rossby radius, so lengths can be scaled on the Rossby radius to collapse all cases on to the $a = 1$ solution. To demonstrate the insensitivity of the trajectories to the initial position, Fig. 2 shows shed vortex trajectories for vortices with different initial conditions which are far further apart than the possible initial error caused by starting along the rigid-lid trajectory. These rapidly relax to the same trajectory. The numerical solution for the vortex trajectory is shown in Fig. 3. Initially, the solution follows the rigid-lid trajectory as predicted. As it moves further from the plate tip, it starts to deviate to its left and continues along a curved trajectory away from the plate tip. The largest difference, however, is the speed of the two solutions. While the distance of the rigid-lid vortex from the plate tip increases like $t^{\frac{2}{3}}$, the distance of the QG vortex from the tip increases like $\log t$. More precisely, Fig. 4 shows that for large time, $1/K_1(\boldsymbol{x}_s) \sim t \sim \Gamma \sim 1/|\dot{\boldsymbol{x}}_s|$, consistent with QGBM equation (10).

B. Free vortex around a semi-infinite plate

The second example considered is a background flow consisting of a free vortex of unit circulation (more general circulations can be recovered through scaling time) moving around a semi-infinite plate, starting at some finite normal distance from the plate but a large distance from the plate tip. Here, the initial distance between the plate and the vortex provides a natural lengthscale so the parameter a stays in the problem and will parameterise a family of solutions.

Fig. 5 shows vortex trajectories for a single free vortex around a semi-infinite plate for various a with no vortex shedding. The vortex is initially far upstream and at unit distance from the plate. The solutions for $a \to 0$ and $a \to \infty$ are exact, and the other solutions are computed using a boundary integral method (the spectral scheme described here reproduces the same results). The rigid-lid

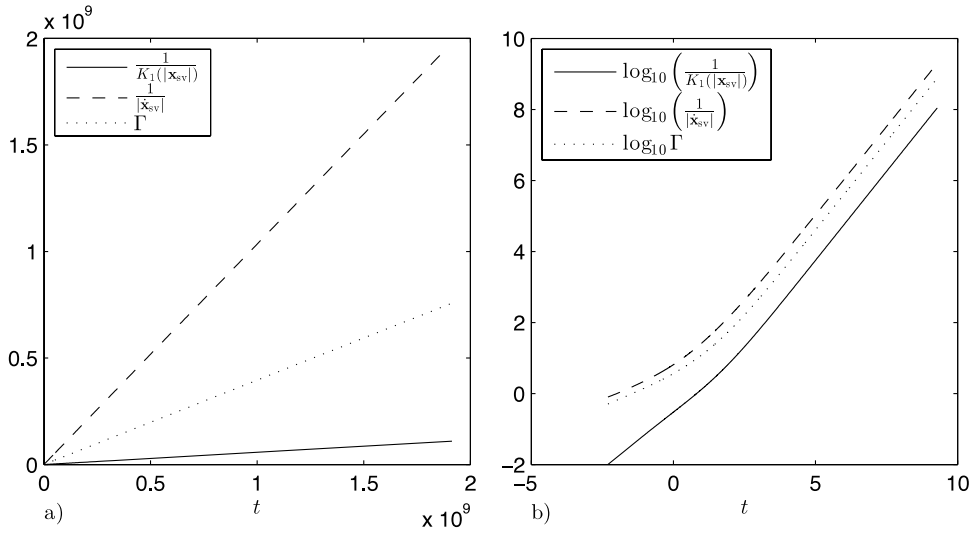

FIG. 4. (a) Standard and (b) log–log plots of $1/K_1(|\boldsymbol{x}_s|)$ (solid), $1/|\dot{\boldsymbol{x}}_s|$ (dashed), and Γ (dotted) against t showing the large time position, velocity, and circulation of a shed vortex in a steady flow around a semi-infinite plate.

solution ($a \to \infty$) can be found by constructing the vortex Hamiltonian in the upper half-plane, then conformally mapping to the semi-infinite plate domain using the known transformation properties of the Hamiltonian under mapping.[38] The trajectory in the limit $a \to 0$ is new and is derived in Appendix B. It is a straight line parallel to the wall from infinity to $x = 0$, then a semi-circular arc around the plate tip then a straight line parallel to the wall again from $x = 0$ back toward infinity, all at constant speed $(\Gamma/2\pi a)K_1(2/a)$, which is exponentially small in $1/a$. All of these solutions pass around the plate tip and get closest to it as they cross the x-axis. The distance of closest approach depends monotonically on a and varies from 0.5 for $a \to \infty$ up to 1 for $a \to 0$.

If flow separation is included, then a second vortex is shed from the plate tip and the two interact. Trajectories for the free and shed vortices are computed for QG flow as before using the spectral method and implicit timestepping described in Sec. III. The coupled ODEs governing the rigid-lid trajectories are found by conformally mapping to the upper half-plane (described in Appendix C) and then integrated using Runge–Kutta timestepping. Fig. 6 shows the trajectories of pairs of free and shed vortices for various a including the rigid-lid limit. For all values of a, instead of the free vortex moving symmetrically around the plate, the two vortices pair up and move off

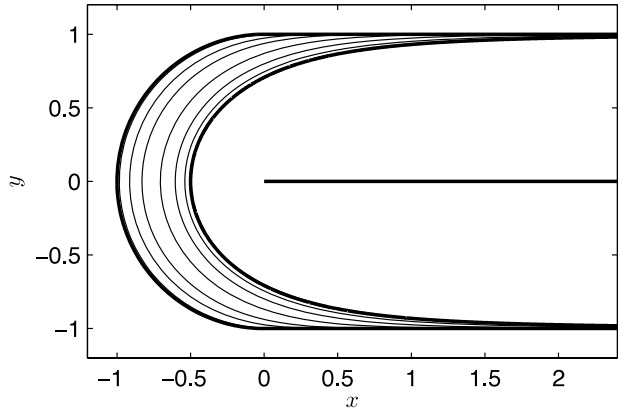

FIG. 5. Free vortex trajectories around a semi-infinite plate, starting from $(x_{f_0}, 1)$ for $x_{f_0} \gg a$, without vortex shedding for (left to right) $a \to 0$ (bold), $a = 0.01$, 0.1, 0.3, 1, 3, 10, and $a \to \infty$ (bold). Bold solutions are exact, and non-bold are computed with a boundary integral method and Runge–Kutta timestepping.

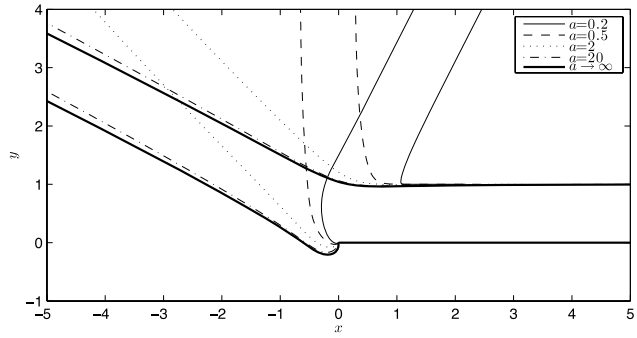

FIG. 6. Trajectories of a free vortex starting from $(x_{f_0}, 1)$ (for $x_{f_0} \gg a$) and a vortex shed from the tip of a semi-infinite plate along the positive x-axis (shown in bold) for $a = 0.2$ (solid), 0.5 (dashed), 2 (dotted), 20 (dash dotted), and $a \to \infty$ (bold). The solution for $a \to \infty$ was computed by integrating the analytically obtained ODEs for the vortex positions with a Runge–Kutta scheme (Appendix C). For finite a, the solutions were computed using the spectral method and implicit timestepping scheme described in Sec. III. The final propagation angle increases monotonically with increasing a.

to infinity along parallel straight trajectories in the upper half-plane. The straight line trajectory is worth remark and implies that the circulation of the shed vortex tends to equal, and opposite sign, that of the free vortex. The eventual angle of propagation (defined as the angle between the ultimate trajectory and positive x-axis) of the pair of vortices increases monotonically with increasing a. The inclusion of flow separation has made a dramatic change to the trajectory: without flow separation, the free vortex moves around the plate symmetrically and ultimately propagates parallel to the plate on the far side and in the opposite direction for all a. With flow separation, the symmetry is broken and the free vortex does not pass around the plate tip and instead ultimately propagates away from the plate in the upper half-plane, with the angle of propagation strongly dependent on a.

The circulation of shed vortices for various values of a is plotted over time in Fig. 7. For all a, the circulation grows from zero to unity, the strength of the free vortex. Fig. 7 shows that, for large a, the circulation grows over the same timescale as the initial movement of the free vortex while, for small a, it grows far quicker. The final separation distance between each pair of vortices and their final angle of propagation is shown in Fig. 8. While the angle is monotonically increasing with a,

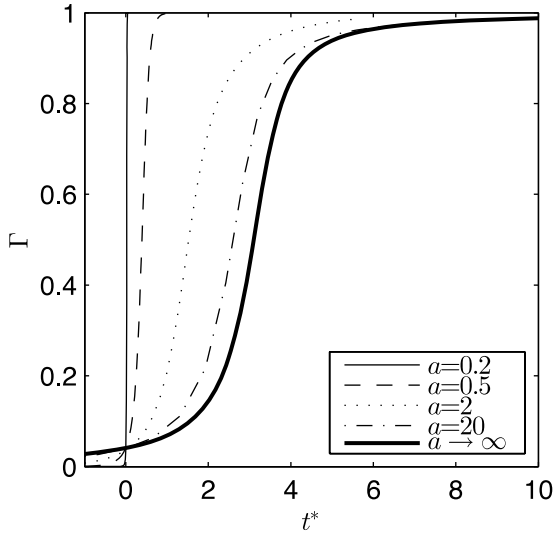

FIG. 7. The circulation Γ of vortices shed from the tip of a semi-infinite plate as a free vortex of unit strength approaches from $(x_{f_0}, 1)$ where $x_{f_0} \gg a$, for various values of a. The circulation is plotted over time t^*, scaled so that in each case the free vortex is initially moving at unit speed, i.e., the scaled time t^* relates to physical time t via $t^* = (2\pi a / K_1(2/a))t$, using the initial speed given by the image of the free vortex in the plate. The curves have been translated so that at $t^* = 0$, they all have the same, small circulation. Therefore, the crossing point of the curves is arbitrary and of no physical importance.

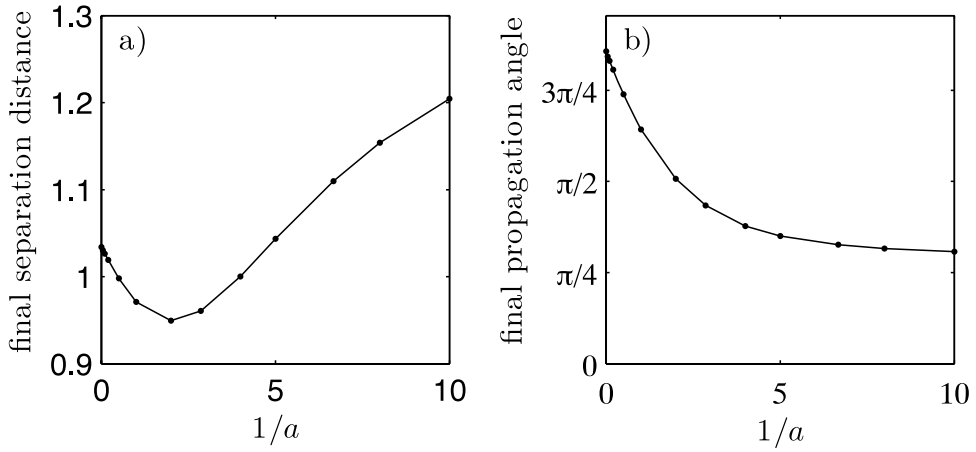

FIG. 8. (a) The final separation distance between each pair of free and shed vortices and (b) their final angle of propagation for varying $1/a$ (to include the $a \to \infty$ result). The separation distance is always significantly smaller than 2—the original separation between the free vortex and its image—so the free vortices are accelerated by shedding. The final propagation angle varies significantly and increases monotonically with increasing a.

the separation distance has a less obvious relationship with a but is always $O(1)$ and less than the initial separation between the free vortex and its image in the plate.

The limit $a \to 0$ is very demanding on the numerical scheme as surface deformations decay over short length scales so high resolution is required, but some progress can be made analytically. According to the method of images, far from the tip the free vortex moves parallel to the wall at speed $K_1(2/a)/2\pi a$ which is exponentially small for small a. Rescaling the vortex strength on $K_1(2/a)/2\pi a$ gives a vortex moving at unit speed. It will have an $O(\mathrm{e}^{(2-|\boldsymbol{x}_\mathrm{f}|)/a})$ effect on the flow at the plate tip. So, in the limit $a \to 0$, the effect at the tip is infinitely small for $|\boldsymbol{x}_\mathrm{f}| > 2$, $O(1)$ for $|\boldsymbol{x}_\mathrm{f}| = 2$, then infinitely large for $|\boldsymbol{x}_\mathrm{f}| < 2$. Thus, it is expected that the shedding will abruptly begin when $|\boldsymbol{x}_\mathrm{f}| = 2$. The shed vortex has negligible effect on the free vortex until it reaches a distance 2 from the plate tip and therefore has comparable strength to the free vortex. At this point, if the vortices are a distance 2 or less from each other, they pair up and move off to infinity on a straight line. Balancing this analysis against the numerical results suggests that the free vortex moves parallel to the wall until it reaches a distance 2 from the tip, at which point the shed vortex is almost instantaneously shed and moves until it reaches a distance 2 from the plate. Then the two move off as a pair at a shallower angle than the $a = 0.1$ solution already computed. Therefore, the free vortex trajectory in the limit $a \to 0$ is expected to be a straight line parallel to the wall up to $|\boldsymbol{x}_\mathrm{f}| = 2$, a sharp turn, then a straight line away again at some angle, conjectured to be around $\pi/4$ based on Fig. 8.

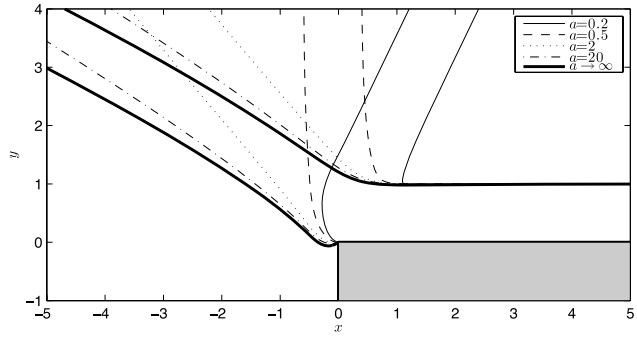

FIG. 9. Trajectories for a free vortex starting at $(x_{\mathrm{f}_0}, 1)$ (for $x_{\mathrm{f}_0} \gg a$), and a Brown-Michael vortex shed from the tip of a wedge of angle $\alpha = \pi/2$ (shown in grey) for $a = 0.2$ (solid), 0.5 (dashed), 2 (dotted), 20 (dash dotted), and $a \to \infty$ (bold). The rigid-lid solution ($a \to \infty$) was computed by numerically integrating the analytically obtained ODEs for the vortex motions as described in Appendix C, and the QG solutions were computed using the method of Sec. III.

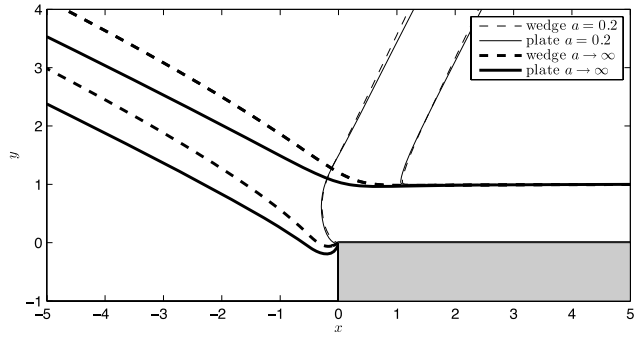

FIG. 10. Comparison of trajectories around a semi-infinite plate and a wedge. Shown are the trajectories of a free and shed vortex around a semi-infinite plate for $a = 0.2$ (solid) and $a \to \infty$ (solid bold) and around a wedge for $a = 0.2$ (dashed) and $a \to \infty$ (dashed bold). For $a = 0.2$, the trajectories for a semi-infinite plate and wedge are very similar whereas for $a \to \infty$, they differ markedly.

C. Free vortex around a right-angled wedge

The third example considered has background flow of a free vortex moving around a right-angled wedge ($\alpha = \pi/2$), starting a finite normal distance from the upper side of the wedge, far from the wedge tip. As it moves around the wedge, a Brown–Michael vortex is shed from the tip of the wedge. Numerically computed solutions (as in Sec. IV B) for the trajectories of the two vortices for various values of a (including the limit $a \to \infty$) are shown in Fig. 9. Similar to the case of a free vortex around a semi-infinite plate, for all a, the free and shed vortices pair up and move away to infinity. Thus, separation has again had a significant effect: the trajectories found are very different to the trajectories of a free vortex around a wedge without the effects of shedding included, which would be symmetrical about a line bisecting the wedge.

The trajectories of a free and shed vortex around a wedge are compared to those around a semi-infinite plate in Fig. 10. For small a, when the trajectories do not pass the wedge tip, the results are very similar. For larger a, when the trajectories do pass the plate tip and therefore are a similar distance from both sides of the wedge, the results differ more significantly. The final propagation angle for the semi-infinite plate trajectory is larger than for the wedge and the large time trajectory is flatter.

V. CONCLUSIONS

The Brown–Michael model is a simplified model which captures the key features of vortex shedding while avoiding both the far more difficult and complex problem of determining the shape and strength of a vortex sheet and the computational cost of a viscous model using a grid-based approach. It has been widely used in a variety of situations to capture the qualitative, and in some cases quantitative, effects of flow separation. A number of comparisons by other researchers of the Brown–Michael model with more sophisticated approaches have shown good qualitative agreement, especially considering its far lower computational cost. Here, it is applied to examine the effects of flow separation from sharply curving boundary topography in the ocean, complementing existing observational, experimental, and more complex numerical work. The original Brown–Michael model is adapted here to better represent mesoscale oceanic flow by including a deforming free surface. This new model has one parameter: the Rossby radius, which is the lengthscale over which surface perturbations decay (infinite Rossby radius being a surface held flat by a rigid-lid). In this work, the effects of vortex shedding and the effect of the Rossby radius are considered for three background flows: a steady flow around a semi-infinite plate (A), a free vortex moving around a semi-infinite plate (B), and a free vortex moving around a right-angled wedge (C). For the steady flow, a vortex is shed from the plate in a similar fashion to rigid-lid flow but slows down exponentially with increasing distance from the tip. This would suggest that, in the ocean, shed eddies are more likely to be found closer to the topography they are shed from than would have been predicted with the original rigid-lid theory. These eddies may be moving slowly enough

to appear trapped. The trajectory of the shed eddy is initially the same as in rigid-lid flow but then deflects away and follows a curved path.

For a free vortex moving around a semi-infinite plate, the inclusion of flow separation significantly changed the vortex trajectory. With no shedding, free vortices for all values of the Rossby radius move around the plate symmetrically, returning in the opposite direction and on the opposite side of the plate from which they approached. With shedding included, and again for all values of the Rossby radius, the shed vortex grew to comparable strength to the free vortex before the free vortex could round the tip and the two moved off as a pair to infinity in the upper half-plane. This result is of significant interest and could merit further investigation. The first step of this should be to test this conclusion against other models such as a vortex sheet method or a model with viscosity explicitly included. If the conclusion is robust, then it would be worth bearing in mind in studies of oceanic flow where there is sharply curved boundary topography but no inclusion of flow separation explicitly or via viscosity.

The Rossby radius has a significant effect on the final propagation direction of the vortex pair. This direction varied by as much as approximately $\pi/2$ between the rigid-lid limit and small Rossby radius results. It is also worth noting that, as for the steady flow, the inclusion of surface deformation slows the vortex but that the vortex pair moves significantly faster than the free vortex moves initially. This acceleration is strongest for the lowest Rossby radius flows. Thus, the inclusion of flow separation not only significantly effects the free vortex trajectory but also accelerates it.

In the case of a free vortex moving around a right-angled wedge, similar results to the semi-infinite plate are found. For all values of a, the free and shed vortices pair up and move off to infinity in the upper half-plane. As with the semi-infinite plate, their final angle of propagation depends monotonically on a. Comparison of trajectories around the wedge and the semi-infinite plate reveals very similar results for low a where the trajectories do not pass the plate tip and therefore are always much closer to the near side of the wedge than the far side. For higher a where the trajectories do pass the plate tip, the results are more different, with the trajectories for the wedge being deflected into the upper half-plane more strongly.

An appealing feature of the original Brown–Michael model and of rigid-lid flow is the wide range of results available analytically. Here, this advantage has been exchanged for a more realistic model, necessitating the development of a non-trivial, bespoke numerical scheme. The method here has been applied to three cases but could relatively straightforwardly be applied to a range more. It is possible to use this model to examine shedding from any shape of boundary topography from which a conformal map to the upper half-plane can be found. An obvious example of interest might be a wall with a gap, in which case two vortices would be shed, one from each edge of the gap. This method could also be used on shapes without sharp corners if there was reason to believe that separation would occur and a separation point could be sensibly specified. For all shapes of boundary topography, a range of background flows could be studied, for example, combinations of time dependent flows and free vortices.

ACKNOWLEDGMENTS

O.R.S. was supported by an EPSRC DTA studentship.

APPENDIX A: $\eta(0, Y) = -\mathrm{erfc}(Y/\sqrt{a})$ FOR STEADY FLOW AROUND A SEMI-INFINITE PLATE

For the case of a semi-infinite plate with background flow with boundary condition on the plate $\eta = -1$, the numerical results indicate that, for $x < 0$, $v(x, 0) = k\mathrm{e}^{x/a}/\sqrt{-ax}$ for some constant k. Integrating this along the negative x-axis and equating to the upstream flux show that the constant $k = -1/\sqrt{\pi}$. As Fig. 11 shows, the numerical results for $v(x,0)$ rapidly converge to $-\mathrm{e}^{x/a}/\sqrt{-a\pi x}$ as N is increased. The streamfunction along the negative x-axis can be found by integrating

$$\eta(x,0) = \int_{-\infty}^{x} \frac{\partial \eta}{\partial x}(x', 0)\,\mathrm{d}x' = \int_{-\infty}^{x} -\frac{\mathrm{e}^{\frac{x'}{a}}}{\sqrt{-\pi a x'}}\,\mathrm{d}x' = -\mathrm{erfc}\left(\sqrt{\frac{x}{a}}\right). \tag{A1}$$

Therefore, in the mapped plane $\eta(0,Y) = -\mathrm{erfc}(Y/\sqrt{a})$.

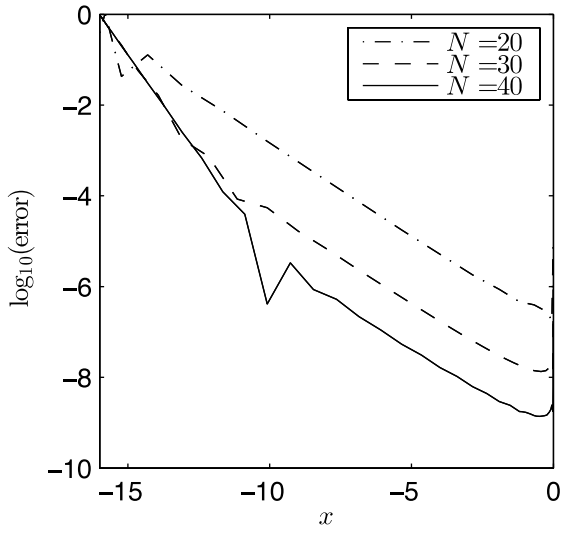

FIG. 11. Log plot of error $= |(-e^x/\sqrt{-\pi x} - v(x,0))/(-e^x/\sqrt{-\pi x})|$, the percentage difference between the numerical solution and suggested exact solution for $v(x,0)$ $(x<0)$ for a steady flow around a semi-infinite plate, plotted over x. Results are shown for $a = 1$ and three different values of N, the number of grid points in each direction in the spectral grid. The numerical solution appears to be converging to the suggested exact solution with increasing N. The influence of the approximate boundary condition at $x = -16$ is also clear but it should be noted both that the solution is exponentially small for large x (the absolute difference between the numerical and suggested exact solutions is approximately 10^{-8} near $x = -16$ for all three values of N plotted here) and that the solution far from the plate tip has exponentially small influence on the flow near the plate tip.

APPENDIX B: VORTEX TRAJECTORY AROUND A SEMI-INFINITE PLATE FOR $a \to 0$

In the limit $a \to 0$, a free vortex moving around a semi-infinite plate with no background flow will only "feel" the effect of the infinitesimal section of boundary closest to it. Therefore, the trajectory of the vortex is a straight line, parallel to the wall until the end of the wall is reached and then a semi-circular arc around the tip until it can again move off parallel to the wall. This can be shown asymptotically by reformulating problem (14) and (15) as an integral equation using the infinite domain Green's function for (14),

$$G(x',y';x,y) = -\frac{1}{2\pi}K_0\left(\frac{\sqrt{(x'-x)^2+(y'-y)^2}}{a}\right). \tag{B1}$$

Applying Green's theorem, $\widetilde{\eta}$ is given by

$$\widetilde{\eta}(x,y) = \iint_{\mathrm{D}} \widetilde{\eta}\,\nabla^2 G - G\nabla^2\widetilde{\eta}\,\mathrm{d}x'\mathrm{d}y' = \underbrace{\int_{\partial\mathrm{D}} \widetilde{\eta}\frac{\partial G}{\partial n}\,\mathrm{d}s}_{\substack{=0\\ \text{as } \widetilde{\eta} \text{ is continuous}\\ \text{across } \partial\mathrm{D}}} - \int_{\partial\mathrm{D}} G\frac{\partial\widetilde{\eta}}{\partial n}\,\mathrm{d}s, \tag{B2}$$

where D is the plane with a wall along the positive x-axis. $\widetilde{\eta}$ can now be expressed in terms of an integral along the plate

$$\widetilde{\eta}(x,y) = -\frac{1}{\pi}\int_0^\infty \left.\frac{\partial\widetilde{\eta}}{\partial y'}\right|_{\substack{x'>0\\ y'=0}} K_0\left(\frac{\sqrt{(x'-x)^2+y^2}}{a}\right)\mathrm{d}x', \tag{B3}$$

in terms of the unknown function $\partial\widetilde{\eta}/\partial y(x,0)$ (for $x>0$). From this, expressions for the velocities $\widetilde{u} = -\partial\widetilde{\eta}/\partial y$ and $\widetilde{v} = \partial\widetilde{\eta}/\partial x$ of the vortex are

$$\begin{pmatrix}\widetilde{u}(x_\mathrm{f},y_\mathrm{f})\\ \widetilde{v}(x_\mathrm{f},y_\mathrm{f})\end{pmatrix} = \frac{1}{\pi a}\int_0^\infty \left.\frac{\partial\widetilde{\eta}}{\partial y'}\right|_{\substack{x'>0\\ y'=0}} \begin{pmatrix}-y_\mathrm{f}\\ x_\mathrm{f}-x'\end{pmatrix}\frac{1}{\sqrt{(x_\mathrm{f}-x')^2+y_\mathrm{f}^2}}K_1\left(\frac{\sqrt{(x'-x_\mathrm{f})^2+y_\mathrm{f}^2}}{a}\right)\mathrm{d}x'. \tag{B4}$$

As $a \to 0$, the integral in (B4) is dominated when the argument of the Bessel function is smallest since the asymptotic form of the Bessel function for large argument r is

$$K_n(r) \sim \sqrt{\frac{\pi}{2r}} \mathrm{e}^{-r} \text{ for } r \gg 1. \tag{B5}$$

When $x_\mathrm{f} > 0$, the argument is minimised by $x' = x_\mathrm{f}$. Therefore, $\widetilde{v} \ll \widetilde{u}$ (as the integrand in $\widetilde{v}$ is equal to 0 at $x' = x_\mathrm{f}$) and the vortex moves parallel to the wall. When $x_\mathrm{f} < 0$, the integrals are dominated by the contribution near $x' = 0$. Hence for some small δ, they may be approximated by

$$\begin{pmatrix} \widetilde{u}(x_\mathrm{f}, y_\mathrm{f}) \\ \widetilde{v}(x_\mathrm{f}, y_\mathrm{f}) \end{pmatrix} \sim \frac{1}{\pi a \sqrt{x_\mathrm{f}^2 + y_\mathrm{f}^2}} \begin{pmatrix} -y_\mathrm{f} \\ x_\mathrm{f} \end{pmatrix} \int_0^\delta \left. \frac{\partial \widetilde{\eta}}{\partial y'} \right|_{\substack{x'>0 \\ y'=0}} K_1 \left(\frac{\sqrt{(x' - x_\mathrm{f})^2 + y_\mathrm{f}^2}}{a} \right) \mathrm{d}x', \tag{B6}$$

so that

$$(x_\mathrm{f}, y_\mathrm{f}) \cdot (\widetilde{u}, \widetilde{v}) = 0, \tag{B7}$$

and the vortex follows a semi-circular trajectory.

In this limit, the movement of the vortex is determined only by the infinitesimally small section of wall closest to it. As the vortex remains a constant distance from this closest section of wall throughout the trajectory, its speed must also be constant. This speed is that given by its image in the wall, $|(\widetilde{u}, \widetilde{v})| = (\Gamma/2\pi a) K_1 (2 y_{\mathrm{f}_0}/a)$, where y_{f_0} is the initial distance from the wall.

APPENDIX C: VORTEX SHEDDING FROM A WEDGE IN THE RIGID-LID LIMIT

In the rigid-lid limit ($a \to \infty$), the ODEs governing the trajectory of a Brown–Michael vortex, shed from the tip of a wedge subject to a flow, are found analytically by mapping to the upper half-plane and constructing the solution by images. These are then integrated using a standard, high-accuracy Runge–Kutta scheme. The procedure is illustrated in this appendix for the case where the background flow is a single free vortex.

Using the mapping shown in Fig. 1, original rigid-lid Brown–Michael equation (12) becomes

$$\frac{\mathrm{d}Z_\mathrm{s}}{\mathrm{d}t} = c^2 |Z_\mathrm{s}|^{-2m} \lim_{Z \to Z_\mathrm{s}} \left(\overline{\frac{\partial \widetilde{W}}{\partial t}} \right) - c Z_\mathrm{s} \frac{\dot{\Gamma}}{\Gamma} \tag{C1}$$

for the shed vortex position in the mapped plane Z_s, where $\widetilde{W}$ is the complex potential for the flow W with the Routh correction for the shed vortex made, i.e.,

$$\widetilde{W}(z) = W(z) + \frac{i\Gamma}{2\pi} \log(Z^{\frac{1}{c}} - Z_\mathrm{s}^{\frac{1}{c}}). \tag{C2}$$

By the method of images, the complex potential when the background flow is a free vortex at $Z = Z_\mathrm{f}$ is

$$W(Z) = -\frac{\mathrm{i}}{2\pi} \left[\Gamma \log \left(\frac{Z - Z_\mathrm{s}}{Z - \overline{Z_\mathrm{s}}} \right) - \log \left(\frac{Z - Z_\mathrm{f}}{Z - \overline{Z_\mathrm{f}}} \right) \right]. \tag{C3}$$

Requiring zero velocity at the origin (i.e., $\mathrm{d}W/\mathrm{d}Z|_{Z=0} = 0$) gives the Kutta condition

$$\Gamma = \frac{|Z_\mathrm{s}|^2 (Z_\mathrm{f} - \overline{Z_\mathrm{f}})}{|Z_\mathrm{f}|^2 (Z_\mathrm{s} - \overline{Z_\mathrm{s}})}. \tag{C4}$$

Differentiating this and substituting it into (C1) gives a pair of complex ODEs in terms of the two complex unknowns Z_s and Z_f which, combined with the standard equation for the evolution of the free vortex position, gives a system which is rapidly and accurately integrated using a fifth-order adaptive timestep Runge–Kutta Dormand–Prince method[37] (MATLAB ode45).

[1] K. Jochumsen, M. Rhein, S. Hüttl-Kabus, and C. W. Böning, "On the propagation and decay of North Brazil current rings," J. Geophys. Res., [Oceans] **115**, C10004, doi:10.1029/2009JC006042 (2010).
[2] H. L. Simmons and D. Nof, "The squeezing of eddies through gaps," J. Phys. Oceanogr. **32**, 314–335 (2002).

[3] C. Cenedese, "Laboratory experiments on mesoscale vortices interacting with two islands," J. Geophys. Res., [Oceans] **110**, C09023, doi:10.1029/2004JC002734 (2005).
[4] M. Duran-Matute and O. U. V. Fuentes, "Passage of a barotropic vortex through a gap," J. Phys. Oceanogr. **38**, 2817–2831 (2008).
[5] P. Richardson, A. Bower, and W. Zenk, "A census of Meddies tracked by floats," Prog. Oceanogr. **45**, 209–250 (2000).
[6] E. R. Johnson and N. R. McDonald, "The motion of a vortex near two circular cylinders," Proc. R. Soc. A **461**, 939–954 (2004).
[7] E. R. Johnson and N. R. McDonald, "The motion of a vortex near a gap in a wall," Phys. Fluids **16**, 462–469 (2004).
[8] E. R. Johnson and N. R. McDonald, "The point island approximation in vortex dynamics," Geophys. Astrophys. Fluid Dyn. **99**, 49–60 (2005).
[9] E. R. Johnson and N. R. McDonald, "Vortices near barriers with multiple gaps," J. Fluid Mech. **531**, 335–358 (2005).
[10] D. G. Crowdy and J. S. Marshall, "Analytical formulae for the Kirchhoff–Routh path function in multiply connected domains," Proc. R. Soc. A **461**, 2477–2501 (2005).
[11] D. G. Crowdy and J. S. Marshall, "The motion of a point vortex around multiple circular islands," Phys. Fluids **17**, 056602 (2005).
[12] D. G. Crowdy and J. S. Marshall, "The motion of a point vortex through gaps in walls," J. Fluid Mech. **551**, 31 (2006).
[13] R. B. Nelson and N. R. McDonald, "Finite area vortex motion on a sphere with impenetrable boundaries," Phys. Fluids **21**, 016602 (2009).
[14] R. S. Nilawar, E. R. Johnson, and N. R. McDonald, "Finite Rossby radius effects on vortex motion near a gap," Phys. Fluids **24**, 066601 (2012).
[15] M. Piedeleu, P. Sangrà, A. Sánchez-Vidal, J. Fabrés, C. Gordo, and A. Calafat, "An observational study of oceanic eddy generation mechanisms by tall deep-water islands (Gran Canaria)," Geophys. Res. Lett. **36**, L14605, doi: 10.1029/2008GL037010 (2009).
[16] O. Isoguchi, M. Shimada, F. Sakaida, and H. Kawamura, "Investigation of Kuroshio-induced cold-core eddy trains in the lee of the Izu Islands using high-resolution satellite images and numerical simulations," Remote Sens. Environ. **113**, 1912–1925 (2009).
[17] M. Jiang, M. Zhou, S. P. Libby, and D. M. Anderson, "Dynamics of a mesoscale eddy off Cape Ann, Massachusetts in May 2005," Deep Sea Res., Part I **58**, 1130–1146 (2011).
[18] T. Takikawa, G. Onitsuka, K.-i. Fukudome, J.-H. Yoon, A. Morimoto, M. Moku, and A. Watanabe, "Spatial and temporal variation of a cyclonic eddy detected downstream of the Tsushima Islands in November 2007," Estuaries Coasts **34**, 775–784 (2011).
[19] K. J. Heywood, D. P. Stevens, and G. R. Bigg, "Eddy formation behind the tropical island of Aldabra," Deep Sea Res., Part I **43**, 555–578 (1996).
[20] I. Andrade, P. Sangrà, S. Hormazabal, and M. Correa-Ramirez, "Island mass effect in the Juan Fernández Archipelago (33S), Southeastern Pacific," Deep Sea Res., Part I **84**, 86–99 (2014).
[21] B. Jiménez, P. Sangrà, and E. Mason, "A numerical study of the relative importance of wind and topographic forcing on oceanic eddy shedding by tall, deep water islands," Ocean Modell. **22**, 146–157 (2008).
[22] S. Teinturier, A. Stegner, H. Didelle, and S. Viboud, "Small-scale instabilities of an island wake flow in a rotating shallow-water layer," Dyn. Atmos. Oceans **49**, 1–24 (2010).
[23] R. M. A. Caldeira and P. Sangrà, "Complex geophysical wake flows," Ocean Dyn. **62**, 683–700 (2012).
[24] C. E. Brown and W. H. Michael, "Effect of leading-edge separation on the lift of a delta wing," J. Aerosp. Sci. **21**, 690 (1954).
[25] R. Krasny, "Desingularization of periodic vortex sheet roll-up," J. Comput. Phys. **65**, 292–313 (1986).
[26] J. M. R. Graham, "The lift on an aerofoil in starting flow," J. Fluid Mech. **133**, 413 (1983).
[27] S. Michelin, S. G. L. Smith, and B. J. Glover, "Vortex shedding model of a flapping flag," J. Fluid Mech. **617**, 1–10 (2008).
[28] S. Michelin and S. G. L. Smith, "An unsteady point vortex method for coupled fluid solid problems," Theor. Comput. Fluid Dyn. **23**, 127–153 (2009).
[29] S. Michelin and S. G. L. Smith, "Falling cards and flapping flags: Understanding fluid solid interactions using an unsteady point vortex model," Theor. Comput. Fluid Dyn. **24**, 195–200 (2010).
[30] J. X. Sheng, A. Ysasi, D. Kolomenskiy, E. Kanso, M. Nitsche, and K. Schneider, "Simulating vortex wakes of flapping plates," *IMA Volume on Natural Locomotion in Fluids and on Surfaces: Swimming, Flying, and Sliding* (Springer, 2012), Vol. 155, pp. 255–262.
[31] J. Eldredge and C. Wang, "High-fidelity simulations and low-order modeling of a rapidly pitching plate," AIAA Paper 2010-4281, 40th AIAA Fluid Dynamics Conference, 2010.
[32] L. Cortelezzi, "On the unsteady separated flow past a semi-infinite plate: Exact solution of the Brown and Michael model, scaling, and universality," Phys. Fluids **7**, 526 (1995).
[33] M. S. Howe, "Emendation of the Brown and Michael equation, with application to sound generation by vortex motion near a half-plane," J. Fluid Mech. **329**, 89–101 (1996).
[34] J. Pedlosky, *Geophysical Fluid Dynamics* (Springer-Verlag, Berlin, 1987), pp. 86–93.
[35] G. K. Batchelor, *An Introduction to Fluid Dynamics* (Cambridge University Press, Cambridge, 1967), pp. 404–407.
[36] C. G. Broyden, "A class of methods for solving nonlinear simultaneous equations," Math. Comput. **19**, 577–577 (1965).
[37] J. Dormand and P. Prince, "A family of embedded Runge–Kutta formulae," J. Comput. Appl. Math. **6**, 19–26 (1980).
[38] P. G. Saffman, *Vortex Dynamics* (Cambridge University Press, Cambridge, 1992), pp. 126–127.